Comparative Study of PMSM with Integer-slot and Fractional-slot Windings

J. A. Güemes, A. M. Iraolagoitia, P. Fernández, M. P. Donsión

Abstract – **This paper examines torque ripple, cogging torque, and radial forces in permanent magnet synchronous motors (PMSMs). Effect of slot number on electromagnetic torque (including cogging torque), and radial forces has been analyzed in different PMSM configurations having the same envelop dimensions and output requirements. Finite element technique is used for computation of the machine characteristics and the electromagnetic forces are calculated using the Maxwell stress method.**

Index Terms— Cogging torque, fractional-slot windings, magnetic forces, PM synchronous motors, torque ripple.

I. INTRODUCTION

PERMANENT magnet synchronous motors (PMSMs) are widely used in many industrial applications for their high efficiency, compact structure, simple mechanical construction and fast dynamic response. As their cost continues to decrease they have the opportunity to become a dominant force in the industrial applications market [1] - [3].

One of the most important problems in permanent magnet motors is the torque ripple which is inherent in their design. This ripple is parasitic, and can lead to mechanical vibration, acoustic noise, and problems in drive systems. Minimizing this ripple is of great importance in the design of PMSMs. Pulsating torque should be specially analyzed for the application of constant speed or high-precision position control, especially at low speed [1]-[2], [4]-[5].

There are three sources of torque ripple coming from the machine: a) cogging torque, b) difference between permeances of the air gap in the d- and q-axis (reluctance torque), and c) distortion of the magnetic flux density waveform in the air gap [6]. Cogging torque is the consequence of interaction (magnetic attraction) between rotor-mounted permanent magnets field and the stator teeth, which produces reluctance variations depending on rotor position; it is independent of stator current. It manifests itself by the tendency of the rotor to align in a number of stable positions even when machine is unexcited, resulting in a pulsating torque which does not contribute to the net effective torque.

In the literature, numerous methods for reducing the cogging torque, such as employing a fractional number of slots per pole, skewing of magnets or stator lamination stack (slots), displacing and shaping the magnets, optimizing the magnet pole-arc-to-pole-pitch ratio, introducing auxiliary slots or teeth, etc, have been proposed [3]-[4], [7]-[12], However, optimizing the cogging torque to a low value is not sufficient to obtain a low torque ripple [3], [10]. As a consequence, in motor design process, the problem of torque ripple reduction should be considered as a whole.

Minimizing torque ripple is of utmost importance in many industrial applications and this is the reason it has received much attention in recent years. Different techniques for torque ripple minimization have been proposed in literature.

Broadly speaking, these techniques can be divided into two main groups.

The first class concentrates on the optimum motor design subject to the constraints of minimum pulsating torque and maximum average torque. Several torque ripple minimization techniques for surface-mounted magnet motors have been proposed [3], [10], [13]-[14]. Use of the same approach for interior-mounted magnet motors is troublesome and imprecise, and is almost absent in literature.

The second class is based on the drive and control concept to generate an appropriate control effort to minimize torque ripple [15]-[19].

The main objective of this paper is to investigate the influence of slot number on torque ripple (including cogging torque) and on radial forces (main causes of magnetic noise) for several 20-pole, three-phase PMSMs with the same envelop dimensions and output requirements.

Finite element technique is used for the computation of the machine characteristics. Core saturation is directly considered in the magnetic field calculation. Maxwell stress method is used to find forces. Implementation can be realized conveniently by using commercially available and technically mature finite element packages.

II. ANALYZED MOTORS

Three-phase, 20-pole PMSMs with 60-, 48- and 24- stator slots are analyzed in this paper. 60 stator slots motor has an integer slot winding and the others have fractional slot windings with 48- and 24-slots. 48- and 24-motors are studied with single-layer and double-layer windings. The analytical calculated fundamental winding factors (k_w) of the machines are: 1 (60 slots), 0.958 (48 slots single layer), 0.925 (48 slots double layer), 0.966 (24 slots single layer) and 0.933 (24 slots double layer). Winding layers are placed horizontally separated at each slot in 48 slot motor, and vertically in 24 slot motor. Total area of all slots, slot opening width, slot height and ampere-turns per phase remains unchanged for all motors. The rotor is the same for all the motors

Cross section of 20-pole, 60-slot PMSM, discussed in this paper, is shown in Fig. 1. Each rotor pole contains a permanent magnet of the neodymium-iron-boron type (NdFeB) that is magnetized across their shorter dimension.

This work was supported in part by the University of the Basque Country under project EHU06/77.

J. A. Güemes, and A. M. Iraolagoitia are with the Electrical Engineering Department, University of the Basque Country, Plaza de la Casilla 3, Bilbao 48012, Spain (e-mail: joseantonio.guemes@ehu.es, ana.iraolagoitia@ehu.es).

P. Fernández is with the Electronics and Telecommunications Department, University of the Basque Country, Plaza de la Casilla 3, Bilbao 48012, Spain (e-mail: pablo.fernandezr@ehu.es).

M. P. Donsión is with the Electrical Engineering Department, Vigo University, Campus of Lagoas-Marcosende, Vigo 36310, Spain (e-mail: donsion@uvigo.es).

978-1-4244-4175-4/10/$25.00 ©2010 IEEE

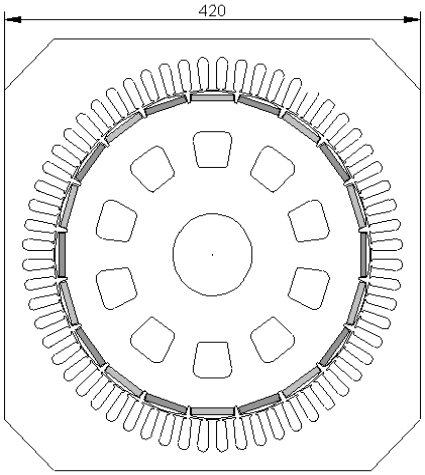

Fig. 1. Cross section 20-pole, 60-slot motor.

Table I shows the main design parameters of the studied motors.

TABLE I
DETAILS OF THE ANALYZED MOTORS

Connection	Star
Frequency of the motor input voltage	15.5 Hz
Power rating (referred to 15.5 Hz)	3 kW
Current rating	10 A
Number of poles	20
Number of stator slots	60/48/24
Number of slots per pole and per phase	1/0.8/0.4
Shaft diameter	80 mm
Stator inner diameter	320 mm
Stator width	420 mm
Stator stack length	80 mm
Magnet pole-arc-to-pole-pitch ratio	0.855
Permanent magnet material	NdFeB
Magnet thickness	5 mm
Width of magnet	42 mm
Coercive magnetizing intensity	920 kA/m
Remanent flux density	1.16 T

III. MODELS AND METHOD

Finite element technique is used for the computation of the machine characteristics. A non-linear field analysis is carried out for calculating the magnetic vector potential and magnetic flux density in each node of the finite element model. In the on load studies, stator winding is excited with three-phase balanced sinusoidal currents to produce the characteristic synchronously rotating magnetomotive force waveform.

Finite element models used are two-dimensional plane. The models are constituted by a transverse section through the middle of the motor (360º geometry). The space of air surrounding the motor has to be taken into account too. The boundary condition is magnetic vector potential null (A = 0) in the periphery of the model. The mesh is more detailed in regions of interest with a sliding mesh in the air gap. Stator mesh remains unchanged and rotor mesh maintains configuration, but changes position following rotor movement.

The electromagnetic forces are calculated using the Maxwell stress method [6], [20]-[22]. This method requires the local flux density distribution along a specific line or contour.

Total force can be calculated by means of the following expression:

$$\boldsymbol{F} = \int_s \frac{1}{2\mu_o}\left(B_n^2 - B_t^2\right) ds\, \boldsymbol{n} + \int_s \frac{1}{\mu_o} B_n B_t\, ds\, \boldsymbol{t} \tag{1}$$

where B_n and B_t, are the normal and tangential components of the magnetic flux density, $\boldsymbol{n}$ and $\boldsymbol{t}$ are the normal and tangential unit vectors to the surface of integration s, and μ_o is permeability of free space.

The normal force is:

$$F_n = \int_s \frac{1}{2\mu_o}\left(B_n^2 - B_t^2\right) ds\, \boldsymbol{n} \tag{2}$$

and tangential force is:

$$F_t = \int_s \frac{1}{\mu_o} B_n B_t\, ds\, \boldsymbol{t} \tag{3}$$

For two-dimensional plane models the integration surface is transformed into a closed contour of radius r (air gap region centre). As the magnetic flux density is calculated at discrete points in the air gap region, the normal and tangential forces in each point of the round path, can be obtained by means of the following expressions:

$$F_n = \frac{B_n^2 - B_t^2}{2\mu_o} d\, l \tag{4}$$

$$F_t = \frac{B_n B_t}{\mu_o} d\, l \tag{5}$$

where d is the length of the path between two consecutive nodes and l is the axial length of the magnetic sheet core.

Taking into account that in rotating electric machine only the tangential component of the Maxwell stresses generates torque, then the torque can be obtained by means of the following expression:

$$T = r\left(\sum \frac{l}{\mu_o} B_n B_t\, d\right) l \tag{6}$$

where r is the radius of the circular path taken.

Forces calculation by means of (4)-(5) depends strongly on the path and mesh structure and a considerable care is required with mesh discretization in the air gap in order to achieve high accuracy. To minimize errors integration contour was established in the middle of air gap with a four-layer mesh (see Fig. 2).

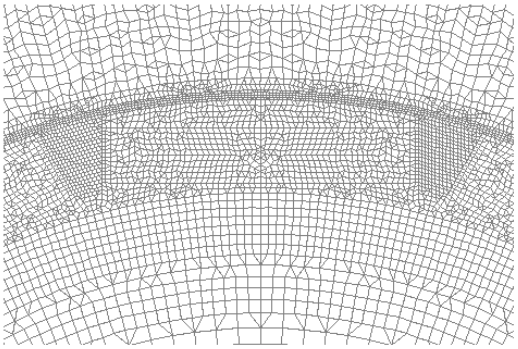

Fig. 2. Two-dimensional meshing model (zoom).

IV. TORQUE

Variation in cogging torque, average torque and torque ripple for the different motors is analyzed in this section.

A. Cogging Torque

The combinations of poles number and slots number of a motor have influence on frequency and peak value of cogging torque waveform.

Two factors can be utilized to find the combinations of number of poles and slots that minimize the cogging torque: first, the number of periods of cogging torque per rotor revolution *(LCM)* or per slot pitch (n_p), and second, the greatest common divisor (*GCD*) between the number of slots (*K*) and number of poles (*2p*).

The number of periods of cogging torque waveform per rotor revolution (n_r) is equal to the least common multiple *(LCM)* between the number of slots *(K)* and number of poles *(2p)*. The number of periods of cogging torque waveform per slot pitch (n_p) can be obtained by means of the following expression:

$$n_p = \frac{LCM(K,2p)}{K} \tag{7}$$

n_r should be as high as possible since a higher number of cogging torque cycles results in smaller peak value. Generally, a high n_r value also has a mitigating effect on the current-dependent ripple torque.

If division between stator slot number and pole number is an integer, only one cogging torque cycle appears per slot and so, cycle number per mechanical revolution is the same than slot number.

Other index for checking the level of cogging torque is the greatest common divisor (*GCD*) between *K* and *2p*. The smaller the *GCD* is less the cogging torque will be.

Table II shows number of slots (*K)*, number of poles (2*p*), number of slots per pole and phase (*q*), slot pitch (p_s), pole pitch (p_p), least common multiple between the pole number and the stator slot number *LCM* (*K,2p)*, number of periods of the cogging torque waveform per slot pitch (n_p) and greatest common divisor between slot number and pole number *GCD*(*K,2p)* for different PMSM configurations analyzed in this paper.

TABLE II
20 POLE MOTORS WITH 60-, 48, AND 24-SLOTS

K	*2p*	*q*	p_s	p_p	*LCM*	n_p	*GCD*
60	20	1.0	6°	18°	60	1	20
48	20	0.8	7.5°	18°	240	5	4
24	20	0.4	15°	18°	120	5	4

To calculate cogging torque, behaviour of the motor for different rotor positions (when there is no current in the windings) is simulated; at each rotor position the meshing is renewed.

Figure 3 shows the cogging torque values as a function of rotor position angle for different motor configurations investigated in this paper. Torque values in 60 slot motor are divided by 50 and divided by 10 in 24-slot motor. It can be seen that cogging torque cycle number in 6 mechanical degrees is: one cycle for 60-slot, four cycles for 48-slot, and two cycles for 24-slot.

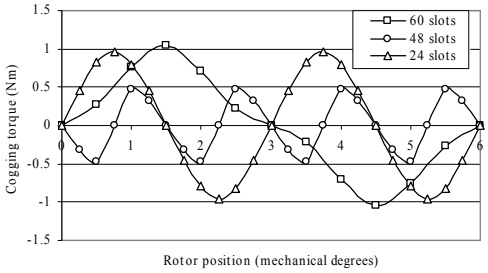

Fig. 3. Cogging torque. Torque values in 60 slot motor are divided by 50 and divided by 10 in 24-slot motor.

Table III shows peak-to-peak value of the cogging torque (T_{cpp}), in analyzed motors.

TABLE III
PEAK-TO-PEAK VALUE OF COGGING TORQUE

Motor	T_{cpp} (Nm)
60 slots	104.5
48 slots	0.9
24 slots	19.2

From these results, it can be seen that: a) maximum cogging torque is obtained in 60 slot motor, and b) peak-peak cogging torque is reduced a 99% and 78.1% for 48 slot motor and 24 slot motor, respectively.

B. Torque Ripple

Electromagnetic torque developed by the motor is calculated simulating on load behaviour of the motor, for different positions of the rotor, when flux armature and excitation are perpendicular ($I_d = 0$, $I_q = I$).

Figure 4 shows the torque ripple as a function of mechanical angle for all analyzed motors. It is clear that torque ripple is smaller in fractional winding motors than in integer winding motor.

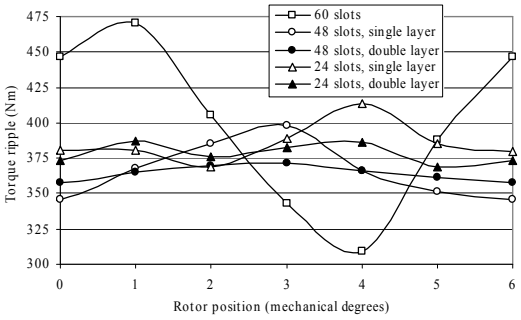

Fig. 4. Torque ripple.

Torque ripple factor (t_r) can been defined as following [6]:

$$t_r = \frac{T_{max} - T_{min}}{T_{av}} \cdot 100 \tag{8}$$

where T_{max}, T_{min} and T_{av} are respectively, maximum, minimum and average values of the torque.

Cogging torque factor (t_c) can be defined as follows:

$$t_c = \frac{T_{cpp}}{T_{av}} \cdot 100 \tag{9}$$

Table IV shows maximum, minimum, average values of the torque (T_{max}, T_{min} and T_{av}, respectively), torque ripple factor (t_r), peak-to-peak value of the cogging torque (T_{cpp}) and cogging torque factor (t_c) for motor configurations analyzed.

TABLE IV
TORQUE RIPPLE FACTOR AND COGGING TORQUE FACTOR

Motor	T_{max} (Nm)	T_{min} (Nm)	T_{av} (Nm)	t_r (%)	T_{cpp} (Nm)	t_c (%)
60 slots	470.2	309.2	393.7	40.9	104.5	26.6
48 slots, S L	398.0	345.9	368.9	14.1	0.9	0.25
48 slots, D L	372	357.4	365.2	4	0.9	0.25
24 slots, S L	413.2	369.1	386.4	11.4	19.2	4.97
24 slots, D L	387.1	369.0	378.9	4.8	19.2	5.07

We can observe that: a) average torque is maximum for 60-slot motor (393.7 Nm) and minimum for 48-slot, double-layer winding motor (365.2 Nm), showing a reduction of 7.2%, b) reduction of average torque is minimum in 24-slot, single-layer winding motor (1.9% compared to the average torque magnitude for 60-slot motor), c) reduction of average torque in 48-slot, single-layer motor and 24-slot, double-layer motor are 6.3% and 3.8%, respectively, compared to the average torque for 60-slot motor, d) torque ripple factor is maximum in 60-slot motor (40.9%) and minimum in 48-slots, double-layer winding motor (4%), e) double-layer winding motors have a slight reduction of average torque (1% in 48-slot motor and 1.9% in 24-slot motor) and higher decrease of torque ripple factor (71.6% in 48-slot motor and 57.9% in 24-slot motor) compared to single-layer winding motors of the same type, and, f) considering only single-layer winding motors, torque ripple factor is minimum for 24-slot motor (this motor shows a higher cogging torque than 48-slot motor). We can observe that optimizing cogging torque to a low value is not enough to ensure a low torque ripple.

V. MAGNETIC NOISE

Vibration and magnetic noise in radial flux electrical machines is due mostly to unbalance of the radial forces [23]-[24]. Radial forces are attractive forces between the stator and the rotor. Irregular magnetomotive force waveforms with fractional-slot windings can cause unbalanced radial magnetic forces.

The greatest common divisor (*GCD*) between the number of poles and the number of slots, indicates that structural periodicity appears around the air gap. It's interesting that *GCD* should be an even number and as high as possible, since this indicates more radial symmetry and good force balance [23].

We can see some contradictions when considering high *GCD* (better balance of radial forces with reduced noise and motor vibrations) or low *GCD* (increment of cogging torque number of cycles per revolution and smaller peak-to-peak value). That means that motor design should try to reach a compromise depending on machine application and operating requirements.

Figures 5 to 9 show the resulting radial magnetic force in the air gap, calculated by means of the equation (4), for all motors analyzed in this paper.

We can observe that: a) 60-slot motor, as expected, shows the greater balance of the radial forces, b) 24-slot, single-layer winding motor has the greatest unbalance (greater vibrations and magnetic noise), and c) analyzed double-layer winding motors have a better balance of magnetic forces than those single-layer winding motor of the same type.

In the previous section, we noticed that double-layer winding motors show a smaller torque ripple than single-layer winding motors. We should notice, though, that double-layer winding manufacturing technique results in higher production costs.

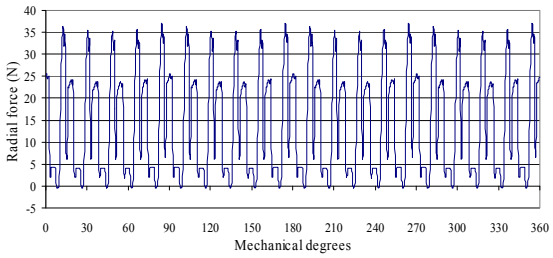

Fig. 5. Radial force by 60 slot motor.

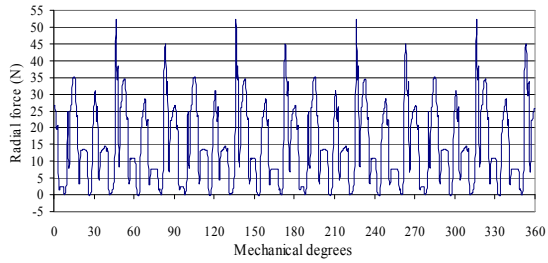

Fig. 6. Radial force by 48 slot motor, single layer.

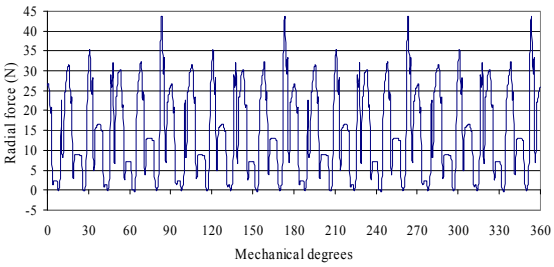

Fig. 7. Radial force by 48 slot motor, double layer.

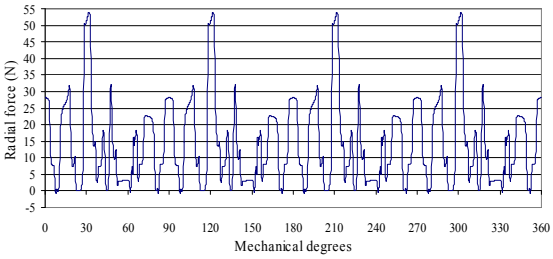

Fig. 8. Radial force by 24 slot motor, single layer.

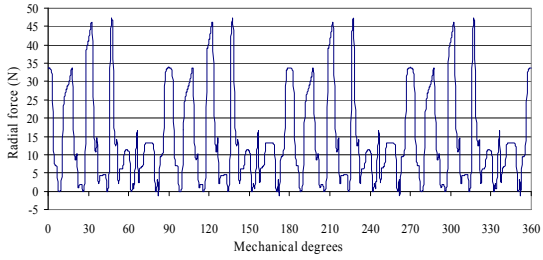

Fig. 9. Radial force by 24 slot motor, double layer.

Figure 10 compares harmonic content of radial magnetic forces (360º mechanical) for all analyzed motors with a theoretical magnetic force waveform of a motor with pure sinusoidal magnetic flux density in the air gap. We observe that: a) theoretical sinusoidal flux density motor (maximum balance of magnetic radial forces) has only constant (0 order harmonic) and 20th harmonic (20 cycles per mechanical revolution), b) 60-slot motor has very small harmonics different from 0 and 20th, and c) higher harmonic content (magnetic noise) appears in the 24-slot, single-layer winding motor. Consequently, even if this motor develops a higher torque than 48 slot motor, we should avoid its use for low-noise applications.

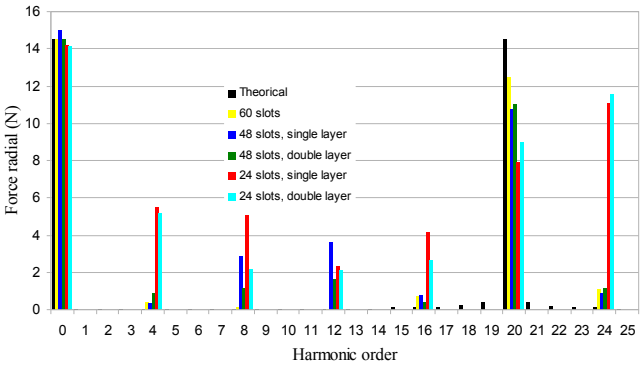

Fig. 10. Amplitude of the radial magnetic force harmonics from the FFT analysis on the FEM-computed radial force.

VI. Magnetic Vector Potential and Magnetic Flux Density

In this section, comparative is made between magnetic vector potential and normal component of magnetic flux density for analyzed motor configurations.

A. Magnetic Vector Potential

Figures 11 to 13 show the air-gap magnetic vector potential waveforms obtained, once the no load and on load analysis of the motors have been carried out. In these figures, horizontal axis represents the position of an observer inside the air gap of the machine. Origin of coordinates corresponds, in all motors, to the beginning of a polar pitch. Simulation results show: a) the strongest deformation of magnetic vector potential waveform in no load, is reached for 24-slot motor (see fig. 11), b) under load conditions, the use of fractional number of slots per pole and phase, increases deformation of the magnetic vector-potential waveform in the air gap of the machine compared with 60-slot motor (integer slot number winding, see Fig. 12), and c) double-layer fractional-slot winding shows a reduction of harmonics content (see Fig. 12 and 13).

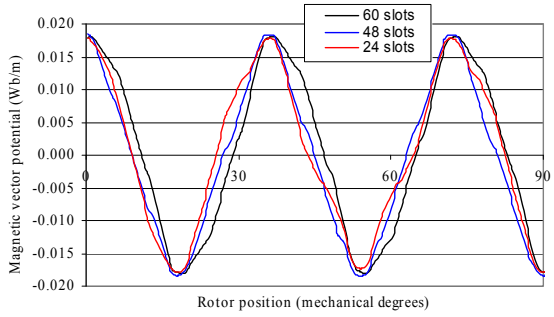

Fig. 11. Magnetic vector potential waveforms in FEM-computed no load test.

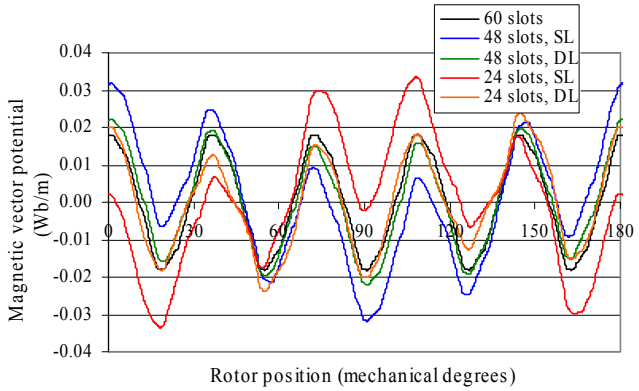

Fig. 12. Magnetic vector potential waveforms in FEM-computed on load test.

Figure 13 shows a comparison of magnetic vector potential waveforms of 60 slot motor and double-layer winding motors, with a theoretical sinusoidal waveform. We can observe that harmonic content increases in 24 slot motor, resulting in larger torque ripple.

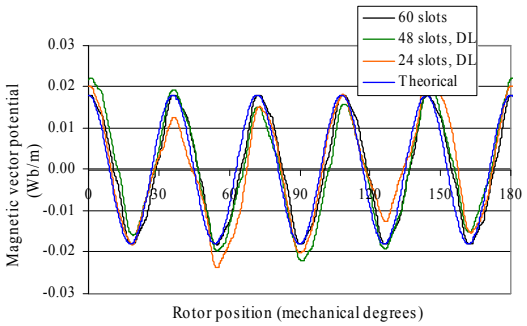

Fig. 13. Magnetic vector potential waveforms in on load test compared with a theoretical sinusoidal waveform.

Comparing results obtained in this section with those from section IV, we can see that for analyzed fractional-slot winding motors, magnetic flux density waveforms in the air gap give a good approach of torque ripple behaviour.

B. Magnetic Flux Density

Figure 14 shows normal component of magnetic flux density in the centre of air gap versus rotor position. From these figure we observe, in accordance with above discussed sections: a) a higher waveform deformation in motors with fractional-slot windings than in motor with integer slot winding per pole and phase and b) double-layer fractional-slot windings show a reduction in flux density waveform harmonics content.

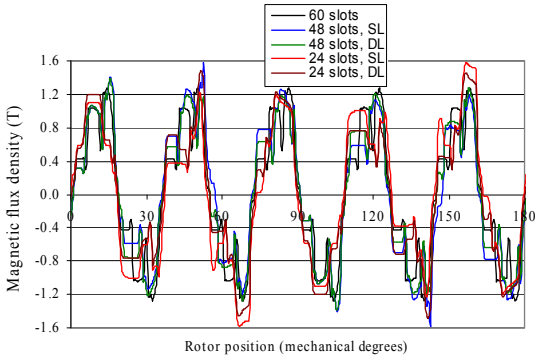

Fig. 14. Normal component of flux density in FEM-computed on load test.

VII. Conclusions

The effect of the slot number on torque ripple (including the cogging torque) has been investigated for five different 20-pole PMSM configurations having the same envelop dimension and output requirements.

Slot and pole number combination and winding type used (single- or double-layer) has a very significant effect on cogging torque, torque ripple and magnetic noise.

Analyzed motors with fractional-slot winding have a lower cogging torque and torque ripple but show a reduction of average torque and unbalanced radial magnetic forces.

48 slot motor shows lower cogging torque than 24 slot motor, but in 24 slot motor using single-layer winding, torque ripple is lower than in 48-slot, single-layer winding motor. We can observe that optimizing cogging torque to a low value is not enough to ensure a low torque ripple.

48-slot, double-layer motor performs the lowest torque ripple of all motors, but also average torque is the lowest.

The highest unbalance of magnetic forces is reached in the 24 slot motors, mostly in single-layer winding.

Analyzed double-layer winding motors show a bigger symmetry of radial forces, smaller torque ripple factor and a slight decrease of average torque, compared to single-layer motors of the same type.

Magnetic flux density normal component and magnetic vector potential distribution along the air gap have been investigated. Assuming a pure sinusoidal phase current distribution, use of fractional number of slots per pole, increases harmonics content of magnetic vector potential, and normal component of the magnetic flux density waveforms. The strongest deformation in magnetic vector potential waveform under no load and on load conditions, is reached for 24-slot, single-layer winding motor.

VIII. REFERENCES

[1] L. Dosiek, and P. Pillay, "Cogging torque reduction in permanent magnet machines," *IEEE Trans. Industry Application*, vol. 43, no. 6, pp. 1656–157, Nov./Dec. 2007.

[2] L. Wu, W. Jin, J. Ni, and J. Ying, "A Cogging torque reduction method for surface mounted permanent magnet motor," *in Proc. International Conference on Electrical Machines and Systems, Seoul – Korea*, 2007, pp. 769–773.

[3] R. Islam, I. Husain, A. Fardoun, and K. McLaughlin, "Permanet-magnet synchronous motor magnet designs with skewing for torque ripple and cogging torque reduction," *IEEE Trans. Industry Applications*, vol. 45, no. 1, pp. 152-160, Jan./Feb. 2009.

[4] Z.Q. Zhu, and D. Howe, "Influence of design parameters on cogging torque in permanent magnet machines," *IEEE Trans. Energy Conversion*, vol. 15, no. 4, pp. 407-412, Dec. 2000.

[5] R. Lateb, N. Takorabet, and F. Meibody-Tabar, "Effect of magnet segmentation on the cogging torque in surface-mounted permanent-magnet motors," *IEEE Trans. Magnetics*, vol. 42, no. 3, pp. 442-445, Mar. 2006.

[6] J. F. Gieras, and M. Wing, *Permanent magnet motor technology. Design and applications*, Marcel Dekker, 2002, pp. 103-104, 246-247.

[7] T. Li, and G. Slemon, "Reduction of cogging torque in PM motors," *IEEE Trans. Magnetics*, vol. 24, no. 6, pp. 2901–2903, 1988.

[8] T. Ishikawa, and G. R. Slemon, "A method of reducing ripple torque in permanent magnet motors without skewing," I*EEE Trans. Magnetics*, vol. 29, no. 2, pp. 2028-2031, Mar.1993.

[9] E. R. Braga, and A. M. N. Lima, "Reducing cogging torque in interior permanent magnet machines without skewing," *IEEE Tran. Magnetics*, vol. 34, no. 5, pp. 3562–3565, Sep. 1998.

[10] P. Salminen, J. Pyrhönen, F. Libert, and J. Soulard, "Torque ripple of permanent magnet machines with concentrated windings," in *Proc. International Symposium on Electromagnetic Fields in Mechatronics, Electrical and Electronic Engineering*, Baiona - Spain, Sep. 2005.

[11] Z..Q. Zhu, S. Ruangsinchaiwanich, and D. Howe, "Synthesis of cogging-torque waveform form analysis of a single stator slot," *IEEE Trans. Industry Applications*, vol. 42, no. 3, pp. 650-657, May/June 2006.

[12] C. Schlensok, M. Herranz-Gracia, and K. Hameyer, "Combined Numerical and Analytical Method for Geometry Optimization of a PM Motor," *IEEE Trans. Magnetics*, vol. 42, no. 4, pp. 1211-1214, Apr. 2006.

[13] C. A. Borghi, D. Casadei, A. Cristofolini, and G. Serra, "Application of a multiobjective minimization technique for reducing the torque ripple in permanent-magnet motors," *IEEE Trans. Magnetics*, vol. 35, no. 5, pp. 4238-4246, Sept. 1999.

[14] C. A. Borghi, D. Casadei, A. Cristofolini, M. Fabbri, and G. Serra, "Minimizing torque ripple in permanent magnet synchronous motors with polymer-bounded magnet," *IEEE Trans. Magnetics*, vol. 38, no. 2, pp. 1371- 1377, Mar. 2002.

[15] W. Qian, S. K. Panda, and J. X. Xu, "Torque ripple minimization in PM synchronous motors using iterative learning control," *IEEE Trans. Power electronics*, vol. 19, no. 2, pp. 272-279, Mar. 2004.

[16] V. Petrović, R. Ortega, A. M. Stanković, and Tandmor, "Design and implementation of an adaptive controller for torque ripple minimization in PM synchonous," *IEEE Trans. Power Electronics*, vol. 15, no. 5, pp. 871-879, Sept. 2000.

[17] J. X. Xu, S. K. Panda, Y. J. Pan, T. H. Lee, and B. H. Lam, "A modular control scheme for PMSM speed control with pulsating torque minimization," *IEEE Trans. Industrial Electronics*, vol. 51, no. 3, pp. 526-536, June 2004.

[18] P. Mattavelli, L. Tubiana, and M. Zigliotto, "Torque-ripple reduction in PM synchronous motor drives using repetitive current control," *IEEE Trans. Power Electronics,* vol. 20, pp. 1423-1431, Nov. 2005.

[19] Y. Abdel-Rady, I. Mohamed, and E. F. El-Saadany, "A current control scheme with an adaptive internal model for torque ripple minimization and robust current regulation in PMSM drive systems," *IEEE Trans. Energy conversion*, vol. 23, no. 1, pp. 92-100, Mar. 2008.

[20] S. Salon, S. Bhatia, and D. Burow, "Some aspects of torque calculations in electrical machines," *IEEE Trans. Magnetics*, vol. 33, no, 2, pp. 2018-2021, Mar. 1997.

[21] J. Mizia, K. Adamiak, A. R., Eastham, and G. E. Dawson, "Finite element force calculation: comparison of methods for electric machines," *IEEE Trans. Magnetics*, vol. 24, no. 1, pp. 447-450, Jan.1988.

[22] W. Zhu, S. Pekarek, B. Fahimi, and B. J. Deken, "Investigation of Force generation in a permanent magnet synchronous machine", *IEEE Trans Energy Conversion*, vol. 22, no. 3, pp. 557-565, Sep. 2007.

[23] F. Magnussen, and H. Lendenmann, "Parasitic Effects in PM Machines With Concentrated Windings", *IEEE transactions on industry applications*, vol. 43, no. 5, pp. 1223-1232, Sep./Oct.2007.

[24] Libert F., Soulard J, "Investigation on Pole-Slot Combinations for Permanent Magnet Machines with Concentrated Windings", *in Pro. International Conference on Electrical Machines*, 5-8 September 2004, Cracow, Poland.

IX. BIOGRAPHIES

J. A. Güemes was born in La Rioja, Spain, in 1952. He received the industrial technical engineering and industrial engineering degrees in electrical engineering, and the Ph.D. degree in industrial engineering from University of Basque Country, Bilbao, Spain, in 1975, 1979, and 1985, respectively.

Currently, he is Full professor of University College with the Electrical Engineering Department, University of the Basque Country, Spain. His research interests include the behavior simulation of grounding grids and the design of devices and electrical machines.

A. M. Iraolagoitia was born in Bilbao, Spain, in 1961. She received the industrial technical engineering and industrial engineering degrees in electrical engineering from University of Basque Country, Bilbao, Spain, in 1983, and 2002, respectively.

Currently, she is Titular Professor of University College with the Electrical Engineering Department, University of the Basque Country, Spain. Her research interests include the design of devices and electrical machines.

P. Fernández was born in Bilbao, Spain, in 1968. He received the industrial engineering degree in electrical engineering, from University of Basque Country, Bilbao, Spain, in 1994.

Currently, he is Titular Professor of University College with the department of electronics and telecommunications, University of the Basque Country, Spain. His research interests include microprocessor design and electrical machine control and design.

M. P. Donsión received his MSc in Industrial Engineering from Catalonian Politechnical University in 1980 and his PhD from Vigo University, Spain, in 1986.

Currently, he is Full Professor with Electrical Engineering Department, University of Vigo, Spain. His main research interests are linked to the: a) Power Quality, b) Renewable Energy with special emphasis in Small Hydro Power and Wind Energy, c) Electrical Machines Modelling, Diagnostics and Control, d) Permanent Magnet Synchronous Motors, and e) Transient Stability of Electrical Power Systems.

He is member of the International Steering Committee of ICEM and member of the Scientific Committee of different conferences, congress and reviews. He is President of the following associations: "European Association for the Development of Renewable Energies, Environment and Power Quality (EA4EPQ)", "European Association for the Development of Electrical Engineering (EADEE)" and "Spanish Association for the Development of Electrical Engineering (AEDIE)", Vice-President of the "Portuguese Association for the Development of Electrical Engineering (APDEE)".